High-Resolution X-ray Structures of Pig Metmyoglobin and Two CD3 Mutants: Mb(Lys^{45}→Arg) and Mb(Lys^{45}→Ser)[†,‡]

Tom J. Oldfield,[§] Stephen J. Smerdon,[*,§] Zbigniew Dauter,[∥] Kyriacos Petratos,[∥] Keith S. Wilson,[∥] and Anthony J. Wilkinson[*,§]

Department of Chemistry, University of York, Heslington, York YO1 5DD, U.K., and EMBL, c/o DESY, Notkestrasse 85, 2000 Hamburg 52, Germany

Received October 7, 1991; Revised Manuscript Received March 23, 1992

ABSTRACT: The structure of pig aquometmyoglobin has been refined to a crystallographic *R*-factor of 19.8% against X-ray diffraction data between 10- and 1.75-Å spacing. The final structural model comprises two molecules of pig myoglobin, 233 water molecules, and two sulfate ions. A water molecule is coordinated to each of the heme iron atoms with an average Fe–OH_2 bond distance of 2.19 Å, and the mean Fe–N_ϵ (proximal histidine-93) distance is 2.20 Å. In contrast to the structure of sperm whale metmyoglobin, the iron is not significantly displaced from the plane of the heme. At the entrance to the heme pocket, the side-chain amino group of lysine-45 (CD3) is well-defined in the electron density map and forms salt-bridging interactions with the heme 6-propionate and with a sulfate ion. Serine and arginine replacements have been made previously at position 45 to examine the proposal that the CD3 side chain acts as a barrier to ligand entry into the protein. Crystal structures of the arginine-45 and serine-45 mutant metmyoglobins have been solved to 1.9 and 2.0 Å resolution, respectively. In both cases the structural changes are confined to the site of mutation. Arginine-45 takes up a conformation closely similar to that observed for this residue in wild-type sperm whale myoglobin, in which it makes more extensive charge–charge and charge–dipole interactions and appears to restrict the movement of the distal histidine away from the ligand. The hydroxyl group of serine-45 is disordered, but it is clear that the effect of the mutation is to open up the solvent-exposed face of the heme pocket.

Structural, kinetic, spectroscopic, and recently, site-directed mutagenesis studies of myoglobin have provided a wealth of information on the heme reactivity and the stereochemistry of ligand binding. What is lacking, however, is a coherent description of the pathway by which the ligand migrates from the bulk solvent to its binding site at the iron within the heme pocket. The iron is recessed some 10 Å in the protein and buried by the polypeptide structure. In the crystal structure, no obvious route of ligand entry is apparent. This is true of both liganded and unliganded myoglobin, indicating that structural fluctuations are an integral part of the ligand binding process and that there is a "gate" which opens transiently to admit the ligand.

Following theoretical molecular dynamics calculations on sperm whale myoglobin, Case and Karplus (1979) proposed a pathway for ligand entry involving passage of the ligand through the solvent-exposed face of the heme into the distal pocket on a trajectory between valine-68 and histidine-64. In their scheme, ligand access was made possible by introducing modest rotations about the side-chain bonds of histidine-64, valine-68, and threonine-67. In subsequent proposals it has been suggested that the imidazole of histidine-64 swings up and away from the iron and out toward the solvent; in doing so, it disrupts one or a number of electrostatic interactions involving arginine-45, the heme 6-propionate, histidine-64 itself, and aspartate-60 on the surface of the protein. Evidence in support of this ligand entry model comes from the crystal structures of myoglobin complexed with bulky ligands (Bolognesi et al., 1982; Ringe et al., 1984; Johnson et al., 1989). For example, in the sperm whale myoglobin–ethyl isocyanide complex, the distal histidine shows disorder indicative of dynamic behavior assuming an "open door" conformation with 45% occupancy. The arginine-45 side chain, which is well-defined in the electron density map, refines to a position (75% occupancy) in which the guanidinium group is pointing outward into the solvent (Johnson et al., 1989). There is also evidence for conformational mobility associated with arginine-45 in the carbonmonoxy structure of sperm whale myoglobin (Kuriyan et al., 1986). In this case, however, the guanidinium moiety points back into the heme pocket in the alternative conformation.

Lysine/arginine residues are conserved at position 45 in all mammalian myoglobins. In the crystal structures, they lie across the front of the heme pocket between the distal histidine and the solvent and form part of the local cluster of groups that interact electrostatically on the protein surface. Of some 60 primary sequences of mammalian myoglobins available, only two, sperm whale and aardvark, contain arginine-45 (Carver et al., 1991). The shorter side chain of lysine-45 appears to offer less hindrance to conformational rearrangements of histidine-64 than arginine, a suggestion which is supported by the observations of Lecomte and LaMar (1985), who measured faster rates of base-catalyzed ^1H exchange of the ring proton of histidine-64 in dog and horse myoglobins, which have lysine-45 than in the sperm whale protein, which has arginine-45.

Rigorous tests of these ligand entry models can be made by substituting side chains implicated in the binding trajectory using site-directed mutagenesis. Kinetic and X-ray crystallographic analyses of the mutant myoglobins can then be

[†] This research was supported by Grant GR/E 98867 from the Science and Engineering Research Council, U.K.

[‡] Crystallographic coordinates have been deposited in the Brookhaven Protein Data Bank for wild-type pig metmyoglobin (1MYG) and the arginine 45 (1MYH) and serine 45 (1MYI) mutant metmyoglobins.

[*] To whom correspondence should be addressed.

[§] University of York.

[∥] EMBL.

0006-2960/92/0431-8732$03.00/0

Table I: Summary of Data Collection and Processing for the Wild-Type and Two Mutant Pig Myoglobins

	wild type	Arg^{45}	Ser^{45}
X-ray source	station X11, DESY[a]	station 9.6, SRS	station X11, DESY[a]
λ (Å)	1.04	0.91	1.04
d_{min} (Å)	1.75	1.9	2.0
$I2_1$ cell parameters	a = 125.3 Å, b = 42.5 Å, c = 92.4 Å β = 92.3°	a = 124.7 Å, b = 42.9 Å, c = 92.8 Å β = 92.9°	a = 125.9 Å, b = 42.9 Å, c = 93.0 Å β = 92.2°
N_{obsd}	98 495 (23 741)[b]	37 845	82 597 (20 492)[d]
R_{merge}[e] (%)	7.8 (6.2)[b]	11.4	5.2 (3.3)[d]
N_{unique}	42 290[c]	27 123	32 815
% complete	92	68	97

[a] Image plate data at DESY were collected as high- and low-resolution data sets. This was achieved by rotating the crystal twice through the same angular range and varying the crystal-to-detector distance and oscillation angle. [b] Two crystals were used in data collection. The first figure quoted is for data (6–1.75 Å) collected from the first crystal rotated about c*; the figure in parentheses is for data collected from the second crystal, which was rotated about a*. [c] Due to complications associated with the handling of overloaded reflections in the wild-type myoglobin image-plate data set during processing, the strongest, mostly low-resolution reflections, were rejected. For this reason, the 6368 reflections from the low-resolution image-plate set, together with the 37 922 and 13 194 reflections from the high-resolution image-plate sets, were merged with 8831 reflections between 100 and 3.0 Å from the data set collected previously on film (Smerdon et al., 1990). These data merge with an R-factor of 6.8%. The number quoted in the table is for this final merged data set. [d] The first number given is for the high-resolution set (10–2.0 Å), and the number in parentheses is for the low-resolution set (100–3.0 Å). [e] See footnote 3.

combined to assess the contributions that individual structural components make to the kinetic barrier to ligand entry (Carver et al., 1990; Carver et al., 1991; Smerdon et al., 1991). As part of these studies and as an extension of our previous X-ray analysis at 2.5-Å resolution (Smerdon et al., 1990), a high-resolution (1.75 Å) structure of wild-type pig myoglobin is presented together with similar resolution structures of two position-45 mutants, Mb(Lys^{45}→Arg) and Mb(Lys^{45}→Ser), that were constructed to probe the role of this residue in ligand binding. Kinetic studies show that substitution of this lysine in pig myoglobin causes small but distinct effects on (i) the kinetics of binding of both ferrous and ferric ligands and (ii) the stability of the protein with respect to autoxidation (Carver et al., 1991; R. Brantley, J. S. Olson, et al., unpublished).

MATERIALS AND METHODS

The purification and crystallization of pig myoglobin have been described elsewhere as have the construction and expression of mutant proteins (Carver et al., 1991; Dodson et al., 1988).

X-ray diffraction data from crystals of wild-type myoglobin and the mutant Mb(Lys^{45}→Ser) were collected at station X11, DESY, on a Fuji imaging plate in combination with a scanning device developed at the EMBL Hamburg outstation (J. Hendrix and A. Lentfer, unpublished). These data were collected as two sets. Initially, all data were measured over a rotation range of 100° in 2° oscillations. Under these conditions, many of the low-resolution terms were saturated. These data were therefore rescued by collecting data over the same rotation range in 5° oscillations, with a longer crystal-to-detector distance. The details and statistics for data collection and processing are shown in Table I.

For the wild-type myoglobin data sets, there were problems in the recording of overloaded intensities which led to the strongest reflections being rejected during processing. Refinement of the wild-type pig myoglobin structure was therefore carried out using data that resulted from merging of the image plate data, collected at DESY, with low-resolution film data (100–3.0 Å) collected previously at station 7.2 at the SRS, Daresbury, U.K. The starting model for refinement was the pig myoglobin structure (Protein Data Bank entry 1PMB, Brookhaven National Laboratory) solved and refined at 2.5-Å resolution (Smerdon et al., 1990). Restrained reciprocal space least-squares refinement procedures (Hendrickson & Konnert, 1979) combined with manual model building into Fourier maps displayed on an Evans & Sutherland PS390 graphics

Table II: Summary of the Restraints Applied during PROLSQ Refinement and the Root Mean Square Deviations from Target Values

	rmsd (Å)	σ
distance restraint		
bond	0.024	0.020
angle	0.068	0.040
planar 1–4	0.085	0.060
plane	0.019	0.020
chiral center	0.157 Å^3	0.120 Å^3
nonbonded		
single torsion	0.238	0.500
multiple torsion	0.231	0.500
possible H-bond	0.236	0.500

device reduced the initial R-factor[1] of 30.2% to 19.8% (all data 10–1.75 Å) with good stereochemistry as shown in Table II. In all, five rebuilds punctuated a total of 79 iterations of the program PROLSQ. Between rebuilds, 2–4 cycles of positional and temperature factor refinement were carried out. A typical cycle comprised five iterations of XYZ and two iterations of XYZ and restrained isotropic B-value refinement. The weighting of the geometrical terms to the X-ray terms was 1.0:0.6. Comparison of the initial and final models revealed an rms (root mean square) shift in main-chain atomic positions of 0.26 Å for each of the molecules of the asymmetric unit with maximum displacements of 0.72 and 1.01 Å for the A and B molecules, respectively.

Refinement of the mutant structures proceeded with the same stereochemical and temperature factor restraints, as well as the same weighting of the geometrical terms to the X-ray terms (1.0 to 0.6) as used for the refinement of the wild-type structure. For Mb(Lys^{45}→Ser), refinement was initiated from the final wild-type model with the CD3[2] side chain included as an alanine and with solvent molecules deleted. Fifty-three iterations of PROLSQ and three rebuilding sessions brought the starting R-factor of 27% down to 19.4% (all data 10–2.0 Å) with acceptable stereochemistry (rms_{bond} = 0.028 Å).

Data from the Mb(Lys^{45}→Arg) mutant crystal were collected at the SRS, Daresbury, U.K., on an Enraf-Nonius FAST television area detector. Following data processing

[1] $R_{cryst} = \sum_{hkl}||F_o| - |F_c||/\sum_{hkl}|F_o|$ where $|F_o|$ and $|F_c|$ are the observed and calculated structure factors of a reflection hkl, respectively.

[2] Nomenclature of Dickerson and Geis (1983).

[3] $R_{merge} = \sum|I_i - I_n|/\sum I_n$ where I_i is an intensity hkl and I_n is the average of the observed equivalents.

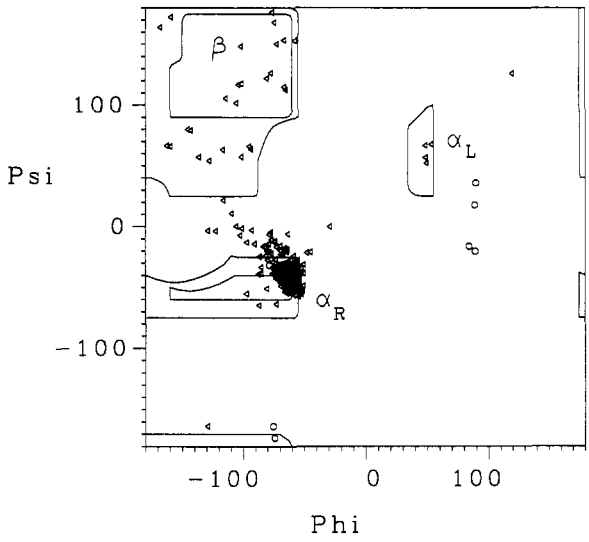

FIGURE 1: Ramachandran plot of main-chain dihedral angles, Φ and Ψ, in degrees for both molecules in the pig wild-type myoglobin asymmetric unit. α_L, α_R, and β indicate the areas associated with left-handed α-helix, right-handed α-helix, and β-sheet conformations, respectively. Glycines are indicated by circles and other residues by triangles.

and reduction, amplitudes were reindexed in the nonstandard monoclinic space group $I2_1$, prior to use in refinement (Smerdon et al., 1990). The starting model was the pig myoglobin structure previously solved and refined at 2.5-Å resolution including 57 water molecules but with the CD3 side chain removed from the phasing (C_β included). Mb-(Lys^{45}→Arg) was initially refined using the restrained molecular dynamics program, XPLOR, implemented on an ALIANT FX-40 minisupercomputer (Brunger, 1988). This lowered the initial *R*-factor of 36.9% to 26.5%, which was reduced further to 23.9% following 20 cycles of PROLSQ refinement and three rebuilds. In the final stages of refinement (8 iterations of PROLSQ), only data with $F > 2\sigma F$ between 7- and 1.8-Å spacing (97% of data measured) were used. The *R*-factor for this model including 96 water molecules and two sulfate ions per asymmetric unit was 22.7% (rms_{bond} = 0.029 Å).

RESULTS AND DISCUSSION

Wild-Type Myoglobin Structure. Overall, the pig myoglobin structure, as expected, is similar to previously reported myoglobin structures with the length and position of the α-helical segments conserved. The Ramachandran plot for the two molecules of the asymmetric unit shows a clustering of main-chain Φ and Ψ angles in the α-helical region (Figure 1; Ramachandran et al., 1963). Besides the glycines (represented by circles), most of the residues which lie outside the allowed areas in Figure 1 are in the "bridge" region, between the α-helical and β-sheet regions. These residues are involved in β-turns in nonhelical segments of the protein. The most conspicuous outliers (in the top right and bottom left of Figure 1), glutamine-152A and glutamine-152B, are very poorly defined in the electron density maps.

Two residues, lysine-79 (EF2) and lysine-98 (FG4), have Φ and Ψ angles which are characteristic of a left-handed α-helical conformation. The equivalent residues in the sperm whale met-, deoxy-, and oxymyoglobin structures also exhibit this feature. Waller and Liddington (1990) have commented on the recurrence of the left-handed α-helical conformation at the FG4 position in hemoglobin and myoglobin. These authors suggest that this unusual conformation is important in maintaining the geometry of the FG corner which, in hemoglobin, is a component of the functionally important $\alpha_1\beta_2$ interface. Evans and Brayer (1990) have reported a type II reverse helical turn conformation at the GH corner between residues 119 and 122, as opposed to the distorted type I reverse turn seen in sperm whale myoglobin at residues 120–123. The main-chain conformations in this region of pig myoglobin are almost identical to sperm whale myoglobin.

The final wild-type pig myoglobin model refined against 1.75-Å resolution data contains 235 water molecules, two sulfate ions, and alternative conformations for seven side chains, glutamine-8A, histidine-48A, lysine-102A, serine-108A, glutamine-8B, lysine-63B, and leucine-89B. The C-terminal residues, glutamine-152 and glycine-153, are disordered. Histidine-48 is involved in an unusual protein–protein contact between the A and B molecules of the asymmetric unit in the pig myoglobin crystal as described in the earlier study (Smerdon et al., 1990). With the higher resolution data, it is apparent that histidine-48A occupies two conformations. In one conformation there appears to be a ring-stacking interaction with histidine-48B, the two residues being related by a pseudocrystallographic 2-fold axis. The N_ϵ of each imidazole makes an intramolecular hydrogen bond to the main chain carbonyl oxygen of lysine-45. In the alternate conformation, the histidine-48A imidazole is rotated by 165° around C_α–C_β toward the solvent approaching C_γ of lysine-45B at a distance of 3.75 Å.

Sperm whale and horse heart myoglobin both crystallize in space group $P2_1$ with one molecule per asymmetric unit (Takano, 1977; Evans & Brayer, 1988) but with different packing arrangements. A sulfate ion is bound at the N-terminus of the E-helix in both crystals, presumably interacting with the α-helix macrodipole as noted previously by Phillips (1980). This sulfate is absent in pig myoglobin, where the close approach of the A and B molecules does not allow the ion to be accommodated. Instead, the sulfate position is occupied by a water molecule. The carboxylate $O_{\epsilon 1}$ of glutamate-54B interacts with the E-helix macrodipole of an adjacent molecule via the peptide nitrogen of glutamate-59A (Figure 2). There is an almost identical interaction between glutamate residues 54A and 59B, which is a consequence of the noncrystallographic 2-fold symmetry. There is a second pair of intermolecular charge–helix macrodipole interactions at the N-terminus of the A-helix involving reciprocal contacts between aspartates 4A and 4B. The mean carboxylate $O_{\delta 1}$ oxygen to main chain amide nitrogen distance is 2.97 Å.

Iron Coordination and Heme Structure. A notable feature of the wild-type pig myoglobin structure, refined against 2.5-Å-resolution data, is the absence in both molecules, in the crystallographic asymmetric unit, of electron density for an iron-coordinated water molecule that would be expected to be present in the ferric form of the protein at neutral pH (Smerdon et al., 1990). Rather, the electron density map reveals a noncovalently bound water molecule that is situated 3.5 Å from the iron and within hydrogen-bonding distance of the distal histidine N_ϵ. In contrast, the 1.75-Å structure described here, refined against data collected from fresh crystals, has water molecules coordinated to the iron atoms of each heme group (Figure 3a and Table III) which are within hydrogen-bonding distance of the N_ϵ atom of the histidine-64 (E7) imidazole. These obvious water peaks in the electron density map give iron–ligand distances of 2.24 and 2.14 Å respectively in the A and B molecules. The unexpected positions observed for the distal pocket water molecules in the earlier study at 2.5-Å resolution remain unexplained.

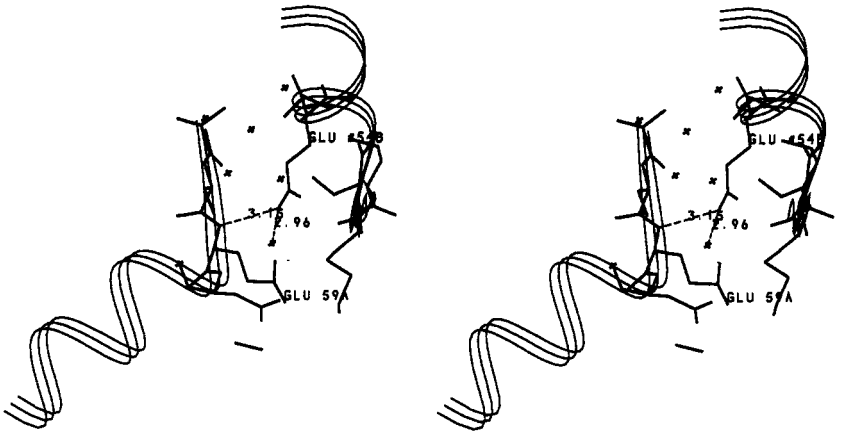

FIGURE 2: Stereopair illustrating the intermolecular contact between the carboxylate group of glutamate-54B and the macrodipole of the E-helix of the A molecule. The position of the water 2.96 Å from the carboxylate of the glutamate corresponds to the position of the sulfate ion seen in the sperm whale $P2_1$ crystal form.

A comparison of the stereochemical details of the heme and ligand-binding site in pig, horse heart, and sperm whale metmyoglobins is presented in Table III (Evans & Brayer, 1990; Takano, 1977). The spin state of the iron in ferric myoglobin changes from pure high spin ($S = {}^5/_2$) at lower pH to an equilibrium thermal mixture of high- and low-spin iron forms at high pH (Antonini & Brunori, 1971; Ozaki et al., 1976). This transition correlates with the ionization of the coordinated water molecule to the hydroxide form. The pK_a for this transition in pig myoglobin, as measured by spectroscopic pH titration, is 8.6 (Biram, 1991). At the pH of crystallization (pH 7.0), it is expected that 97.5% of the iron atoms will be in the high-spin form. It is evident that the heme iron is not significantly displaced from the least-squares plane of the pyrrole nitrogen atoms in either the horse or pig myoglobin crystal structures. In contrast, the iron is displaced by 0.27 Å in the sperm whale metmyoglobin structure refined against 2.0-Å data using real-space least-squares minimization procedures (Takano, 1977). In a later sperm whale metmyoglobin structure refined by reciprocal-space least-squares methods against 2-Å-resolution data, the displacement of the iron was reported to be 0.18 Å (Kuriyan, 1986; Kuriyan et al., 1986). Large displacements of the iron from the plane of the pyrrole nitrogens are also seen in the X-ray structures of ferric heme complexes such as chlorohemin (a 5-coordinated iron displaced from the plane 0.5 Å toward the chloride ligand) and methoxy-substituted iron(III) mesoporphyrin IX dimethyl ester (Koenig, 1965; Hoard et al., 1965).

The heme is distorted in both molecules of the pig myoglobin asymmetric unit. In particular, pyrroles C and D are noticeably inclined to the least-squares plane of the heme, with the pyrrole nitrogens pointing toward the proximal side of the heme group. These distortions may be due to the high-spin iron being too large to fit among the pyrrole nitrogens of a perfectly flat heme. The Fe–OH_2 bond lengths in both the pig and horse myoglobin structures are slightly longer than in sperm whale myoglobin. This is probably due to the different methods of refinement used in the two studies and to the fact that this bond length was constrained in the earlier sperm whale myoglobin work.

The final ($F_o - F_c$) map contains positive features, in both molecules of the asymmetric unit between the iron atom and the nitrogens (N_p) of pyrroles A and C, indicative of anisotropy in the thermal vibration of the iron which was not accounted for in the isotropic temperature factor refinement (Figure 3b). This density cannot be the result of lattice disorder as the vectors joining the nitrogens of pyrroles A and C in the two molecules of the asymmetric unit are not collinear. It is unlikely that this effect is due to absorption or anomalous scattering from the iron (ignored during data processing) since the wavelength of radiation used during data collection (1.04 Å) is far from the iron absorption edge ($\lambda_{K_{abs}} = 1.7435$ Å).

As is evident from Figure 3b, the plane of the imidazole of histidine-93 lies almost exactly along the equatorial Fe–N_p bonds between pyrroles A and C. This is sterically the least-favored conformation since it brings the imidazole ring carbons C_ϵ and C_δ within 3.10 and 3.09 Å of the nitrogens of pyrroles A and C, respectively. Eclipsed conformations of imidazole ligands of iron porphyrins prevail in the X-ray structures of both model heme compounds and in myoglobins and hemoglobins from a number of species. An exception is leghemoglobin where the imidazole adopts a staggered conformation. Charge iterative extended Huckel calculations have suggested that favorable π-bonding effects between the porphyrin iron and the imidazole nitrogen can account for the preference for eclipsed conformations (Scheidt & Chipman, 1986). In myoglobin, the orientation of the imidazole is also influenced by two hydrogen-bonding interactions made by N_δ with the main chain C=O of leucine-89 and the O_γ of serine-92 (F7). The serine-92 O_γ is in turn involved in a complex hydrogen-bonding network involving the heme propionic acid, histidine-97, and solvent. It is notable that residue F7 is either serine or threonine in all mammalian myoglobins sequenced to date, while in human hemoglobin, it is a leucine in both the α and β subunits and variable in hemoglobins from other species. The functional significance of this interaction is being tested by site-directed mutagenesis of pig myoglobin and reciprocal experiments in human hemoglobin.

Heme Pocket and Lysine-45. A large peak in the ($2F_o - F_c$) Fourier map, situated at the entrance to the distal pocket, was initially modeled as a water molecule. In the later cycles of refinement, a sulfate ion was refined at this position to account for the size and shape of the peak and for the density observed in $F_o - F_c$ Fourier maps tetrahedrally distributed about the water position (Figure 3c). This sulfate makes chemically sensible contacts with lysine-45 (N_ζ–O = 3.8 and 3.2 Å), histidine-64 (N_δ–O = 2.4 and 2.4 Å), and threonine-67 (O_γ–O = 3.0 and 2.8 Å) though it may not be present at full occupancy. The close contact made between the N_δ of the histidine-64 side chain and the sulfate oxygen suggests strongly that the imidazole is protonated at N_δ. This implies either that the side chain is ionized or that the N_ϵ acts as a hydrogen bond acceptor in its stabilizing interaction with the iron-coordinated water molecule. The position of this sulfate

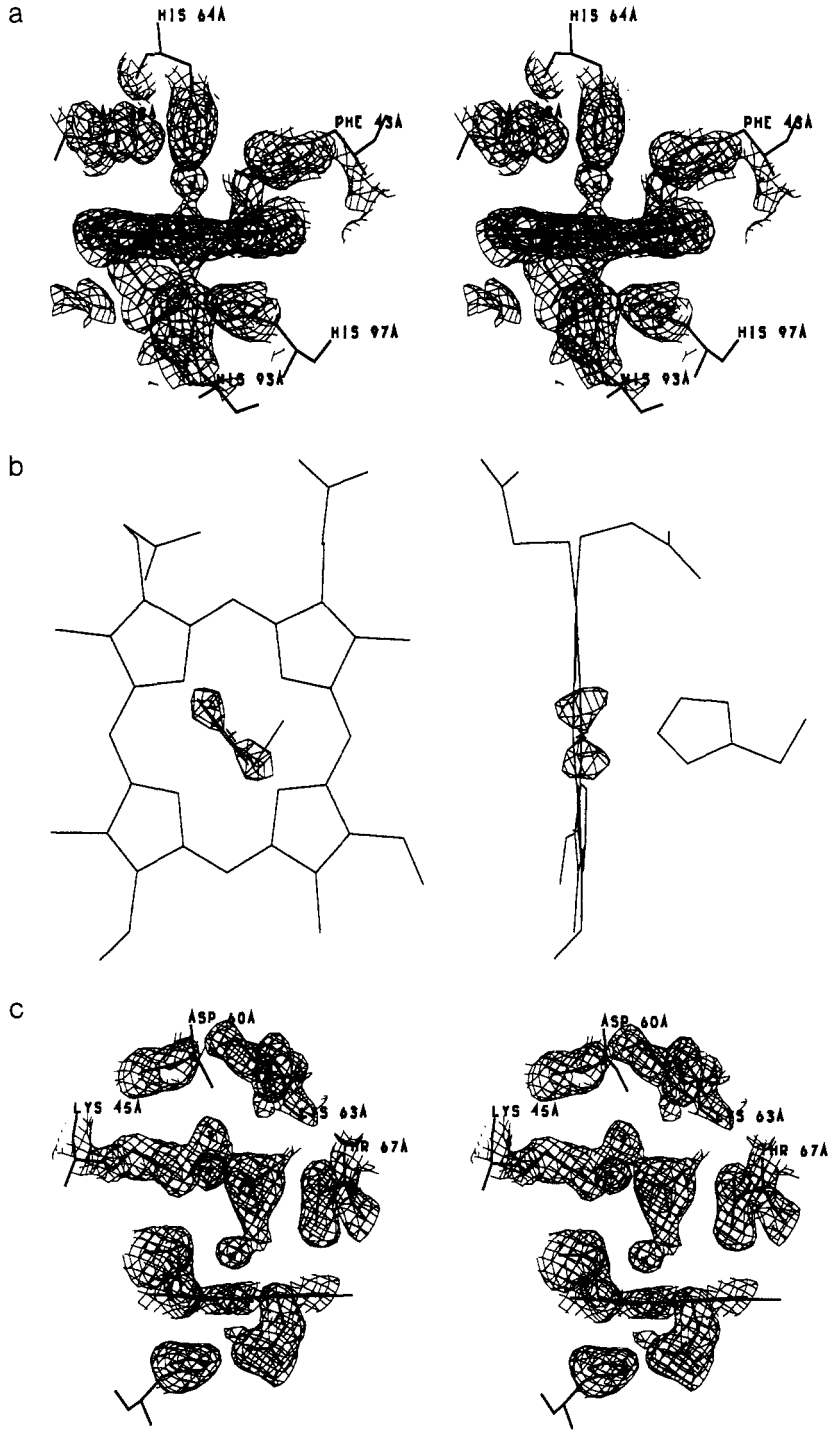

FIGURE 3: (a) Stereopair of the $2F_o - F_c$ Fourier synthesis contoured at 2σ (0.90 e/Å^3) for the heme environment in the wild-type structure (A molecule) viewed from the rear of the heme pocket. The positions of the distal histidine-64, valine-68, phenylalanine-43, and iron-coordinated water molecule in the distal pocket together with the coordinating histidine-93 (F8) and histidine-97 on the proximal side of the heme are shown. (b) Orthogonal views of the heme group in the wild-type structure (B molecule). A portion of the final $(F_o - F_c)$ map contoured at 3.5σ (+0.28 e/Å^3) showing positive features around the heme iron is superimposed. The proximal histidine-93 is also shown. Distortion of the D pyrrole is evident. (c) Stereoview of the $2F_o - F_c$ Fourier synthesis contoured at σ (0.45 e/Å^3) showing the relative conformations of lysine-45, aspartate-60, lysine-63, threonine-67, the bound sulfate ion, and solvent structure around the heme pocket entrance of the A molecule. Histidine-64 has been omitted for clarity.

ion is similar to that observed in the X-ray structure of sperm whale metmyoglobin (Takano, 1977). It is not present in the structure of recombinant sperm whale myoglobin purified from *Escherichia coli*, also crystallized from ammonium sulfate but in the hexagonal space group, *P*6, at pH 9.0 (Phillips et al., 1990), or in the horse heart metmyoglobin structure (Evans & Brayer, 1990), which indicates that the presence or absence of this sulfate ion is dependent on the conformation and charge of surrounding side chains, the charge on the heme iron (ferrous structures contain no sulfate at the heme pocket entrance), and also the molecular packing in the crystal. The heme pockets of both molecules in the pig myoglobin asymmetric unit face a large solvent channel in the crystal lattice (Smerdon et al., 1990). Thus, it is reasonable to suppose that side-chain conformations in this region of the molecule are unaffected by lattice contacts between symmetry-related molecules.

Lysine-45 is well-defined in both molecules. The terminal N_ζ atoms reside at distances of 3.59 and 3.54 Å from the heme

Table III: Comparison of the Heme Geometry and Stereochemistry for Pig, Sperm Whale, and Horse Aquometmyoglobins

distance (Å)	pig Mb (A)	pig Mb (B)	horse Mb[a]	SW Mb[b]
Fe–plane of pyrrole nitrogens	–0.04	–0.07 (–0.055)[c]	–0.03	0.27
His^{93} (F8) Fe–N_ϵ	2.22	2.18 (2.20)	2.26	2.13
Fe–pyrrole N (av)	2.02	2.00 (2.01)		2.04
Fe–H_2O	2.24[d]	2.14[d] (2.19)	2.29	2.00 (constrained)

[a] Data taken from Evans and Brayer (1990). [b] Data taken from Takano (1977). [c] Distances in parentheses are the averages of the A and B molecules in the pig myoglobin asymmetric unit. [d] Unrestrained.

6-propionic acid carboxylate oxygen atoms in the A and B molecules, respectively. This distance is somewhat greater than the arginine-45–propionate distance in sperm whale metmyoglobin (N_η–O_{prop} = 2.93 Å) and may account for the slower rates of heme reorientation (so-called "hopping" around the histidine-93–Fe bond) observed in the sperm whale protein than in myoglobins with lysine-45 (LaMar et al., 1991). It is now clear that lysine-45 is far removed from aspartate-60 (6 Å), explaining why the pig mutant Mb(Asp^{60}→Ser) (Carver et al., 1991) has unaltered ligand-binding kinetics. Lambright et al. (1989) have constructed a human myoglobin mutant Mb(Asp^{60}→Glu). Glutamate-60 could, in principle, make contact with CD3 lysine, but even in this case, no effect on the association rate for CO binding was observed.

Mb(Lys^{45}→Arg). The lysine-45 to arginine myoglobin mutant was constructed to examine the effects of introducing extra bulk and hydrogen-bonding potential at the entrance to the heme pocket and to mimic the arrangement observed in sperm whale myoglobin. As is evident from Table I, the X-ray data for this mutant crystal are both of poorer quality and incomplete. In spite of this and the high *R*-factor, arginine-45 is well-defined in the final ($2F_o - F_c$) Fourier map as shown in Figure 4a. The conformation of the side chain is similar to that observed for arginine-45 in the sperm whale protein. The guanidinium group is in a position to make a salt bridge to the heme 6-propionate (2.6 and 2.6 Å) and to one of the carboxyl oxygens of aspartate-60 (3.1 and 3.0 Å). Aspartate-60 adopts a conformation different from that observed in the sperm whale protein (Figure 4b), where an additional hydrogen bond (2.8 Å) is apparently formed between the N_ϵ of the guanidinium group and the second carboxyl oxygen of aspartate-60. This is a consequence of 52° and 20° relative rotations of the aspartate side chain about its C_α–C_β and C_β–C_γ bonds, respectively, in the sperm whale structure (Figure 4b). Hubbard et al. (1990) have recently reported the structure of a human myoglobin mutant Mb(Lys^{45}→Arg) at 2.8-Å resolution in which aspartate-60 adopts a conformation similar to that observed in the sperm whale protein. There is no sulfate ion at the heme pocket entrance in the human Arg^{45} mutant, in contrast to sperm whale myoglobin, which naturally has arginine at position 45. For pig Mb(Lys^{45}→Arg), we believe that the sulfate ion, present in the wild-type protein, persists. A water molecule could not be satisfactorily refined into the electron density peak at the entrance to the heme pocket. In the later stages of refinement, therefore, a sulfate ion was placed at this position to account for the size of the observed peak. The differences between the pig and human mutant structures may be attributable to the proximity of residues involved in crystal contacts in the human myoglobin mutant crystal form.

Ligand-binding experiments show that pig and sperm whale myoglobins have closely similar affinities for oxygen and carbon monoxide (Carver et al., 1991). It is surprising, therefore, that the effect of the conservative arginine for lysine replacement in pig myoglobin is to increase the O_2 and CO affinities 2–4-fold. Kinetic measurements also show that CO binds more rapidly to the mutant than to wild-type pig myoglobin despite the bulkier CD3 side chain. More detailed analysis suggests that the rate of the bimolecular process of ligand entry into the heme pocket is unchanged, and that it is the rate of unimolecular binding to the iron from within the heme pocket that is accelerated (Carver et al., 1991). There is no evidence from the maps to suggest that the position of the iron atom has changed as a consequence of mutation. The increased reactivity of the mutant may therefore be the consequence of secondary effects of the position-45 side chain mediated through interactions with the histidine-64 imidazole or the heme 6-propionate; however, it is not possible to attribute the cause of these kinetic differences directly to specific features in our crystal structures.

The lower affinity and slower rates observed for wild-type (arginine-45) sperm whale myoglobin (relative to the arginine-45 mutant pig myoglobin) may be related to the difference in the position of the iron atom with respect to the least-squares plane of the pyrrole nitrogens observed in the aquomet structure (Table III). Thus, the out-of-plane, and presumably less reactive, iron in sperm whale myoglobin could compensate for the increased reactivity conferred by the arginine residue at CD3. The structural changes responsible for the out-of-plane iron are not readily discernible but are perhaps reflected in the rms difference in main-chain atomic positions of the least squares matched pig mutant and sperm whale models of 0.6 Å compared with the rms difference between pig Mb(Lys^{45}→Arg) and the pig wild-type protein of only 0.3 Å.

Mb(Lys^{45}→Ser). In order to test the effects of removal of the interactions between the CD3 side chain and both the heme 6-propionate and histidine-64, lysine-45 was substituted with serine. The quality of the overall electron density map for Mb(Lys^{45}→Ser) is good, consistent with the quality of the X-ray diffraction data from these crystals (Figure 5, Table I). A water site near serine-45A was identified during the course of refinement, situated between O_γ and the carboxylate group of aspartate-60 (Figure 5). The O_γ was modeled so as to make a hydrogen bond with the new solvent molecule. This water is, however, absent in the B molecule, and the electron density associated with the serine-45B side chain indicates that the terminal OH group is disordered. It is our impression that the sulfate ion present in both the wild-type and Mb(Lys^{45}→Arg) structures is absent or, at best, present at much lower occupancy in this mutant, consistent with the loss of positive charge at the heme pocket entrance. Elsewhere the structure of Mb(Lys^{45}→Ser) shows only small deviations from that of the wild-type protein as is evident from the rms shifts of 0.25 Å for overlap of the main-chain atoms (residues 5–145) of the asymmetric unit and 0.13 and 0.13 Å for overlaps of the A and B molecules individually. This indicates a small rigid body movement of one molecule of the asymmetric unit with respect to the other, as has been observed in the structure of a previously reported pig myoglobin mutant (Smerdon et al., 1991).

Replacement of lysine-45 with a small polar (serine) side chain results in a more accessible ligand-binding pocket. Rotation of the histidine-64 "gate" is no longer hindered by the CD3 side chain (Figure 5). No significant differences in the temperature factors associated with the distal histidine side chain are observed, suggesting that removal of the lysine side chain does not bestow any increased mobility on the histidine-64 imidazole. However, in the aquomet ligation state

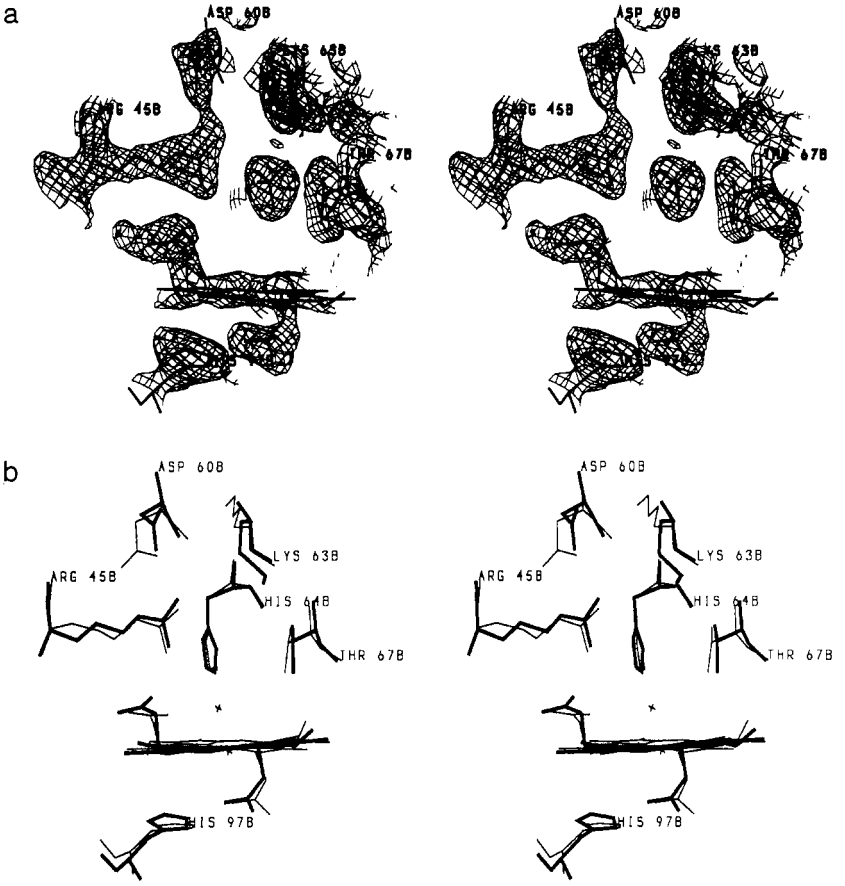

FIGURE 4: (a) Stereoview of the $2F_o - F_c$ Fourier synthesis contoured at σ (0.51 e/Å^3) showing the arrangement of the residues at the heme pocket entrance in the Mb(Lys^{45}→Arg) structure. Histidine-64 has been omitted for clarity. (b) Stereosuperposition of heme pocket residues of the pig arginine-45 mutant structure (thick lines) and the wild-type sperm whale myoglobin structure (thin lines). The least-squares overlap was carried out with the main-chain atoms of residues 2–150 of the Mb(Lys^{45}→Arg) B molecule. The heme environment is represented, and the relative conformations of the aspartate-60 carboxylate are apparent. The rms difference for main-chain atomic positions is 0.6 Å.

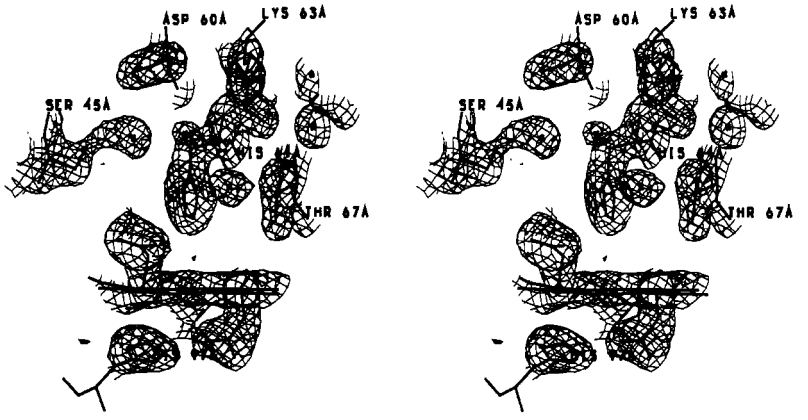

FIGURE 5: Stereoview of the $2F_o - F_c$ Fourier synthesis contoured at 1.2σ (0.61 e/Å^3) showing the arrangement of the residues at the heme pocket entrance in the Mb(Lys^{45}→Ser) structure. The water molecule within hydrogen-bonding distance of the O_γ of serine-45A is not present in the B molecule. Histidine-64 is apparently less restricted than in the wild-type or (Lys^{45}→Arg) protein.

the histidine side chain is hydrogen-bonded to the iron-bound water molecule, which presumably restricts its mobility relative to the 5-coordinate deoxy form.

Despite the more open pocket structure seen in Mb(Lys^{45}→Ser), there are no changes in the rates of association of the diatomic ligands, O_2 and CO, suggesting either that lysine-45 is not a kinetic barrier to the proposed motion of the distal histidine side chain or that the ligand enters via a different channel whose formation does not involve significant structural rearrangement at the front of the heme pocket (Carver et al., 1991). There are 2-fold increases in the equilibrium constants for the binding of alkyl isocyanides to this mutant, brought about through increases in the association rate constants. Bound isocyanide ligands cause steric crowding in the heme pocket, as the displaced conformations of histidine-64 and arginine-45 in the sperm whale myoglobin ethyl isocyanide complex attest (Johnson et al., 1989). When lysine or arginine is replaced by serine-45, no displacement of the CD3 side chain is required for isocyanide association.

Conclusions. The crystal structures of the mutant myoglobins confirm that no gross structural changes accompany the substitutions of the highly conserved CD3 residue in myoglobin. From the Mb(Lys^{45}→Ser) studies, it appears that a positively charged residue at CD3 is not a critical

determinant either of the structural integrity of myoglobin or of its ligand-binding properties (Carver et al., 1991). It may instead have a key role in the binding of heme or in the interaction of the protein with the metmyoglobin reductase system, which have not as yet been investigated.

Accurately determined crystal structures of mutant proteins are often valuable for understanding how amino acid substitutions in proteins influence the functional properties of the molecule. It is arguable that the insights these structures can provide are limited when, as is the case in this study, the phenomenon being investigated is exquisitely related to the solution dynamics of the protein. Refined crystal structures do contribute indirectly, however, toward the elucidation of the pathway of ligand entry into the protein by extending the basis for further molecular calculations.

ACKNOWLEDGMENT

We thank Glaxo, U.K., for the use of computing facilities at York; Rod Hubbard, Paul Holden, Alex Cameron, and Eleanor Dodson for help with data processing; and Professors John Olson and Guy Dodson for helpful discussions and critical reading of the manuscript.

REFERENCES

Antonini, E., & Brunori, M. (1971) *Haemoglobin and Myoglobin in their reactions with ligands*, Elsevier North-Holland, Amsterdam.

Biram, D. (1991) Ph.D Dissertation, University of York, York, U.K.

Bolognesi, M., Cannillo, E., Ascenzi, P., Giacometti, G. M., Merli, A., & Brunori, M. (1982) *J. Mol. Biol. 158*, 305–15.

Brunger, A. T. (1988) *J. Mol. Biol. 203*, 803–16.

Carver, T. E., Rohlfs, R. J., Olson, J. S., Gibson, Q. H., Blackmore, R. S., Springer, B. A., & Sligar, S. G. (1990) *J. Biol. Chem. 265*, 20007–20.

Carver, T. E., Olson, J. S., Smerdon, S. J., Krzywda, S., Wilkinson, A. J., Gibson, Q. H., Blackmore, R. S., Dez Ropp, J., & Sligar, S. G. (1991) *Biochemistry 30*, 4697–705.

Case, D. A., & Karplus, M. (1979) *J. Mol. Biol. 132*, 343–68.

Dickerson, R. E., & Geis, I. (1983) in *Haemoglobin: Structure, Function, Evolution and Pathology*, Benjamin/Cummings, Menlo Park, CA.

Dodson, G. G., Hubbard, R. E., Oldfield, T. J., Smerdon, S. J., & Wilkinson, A. J. (1988) *Protein Eng. 2*, 233–7.

Elber, R. (1990) Simulation of Ligand Diffusion in Myoglobin and Myoglobin Mutants, in *Research Summaries for Fogarty International Center Conference on the Dynamics and Kinetics of Myoglobin and Haemoglobin* (Brunori, M., Eaton, W. A., Gibson, Q. H., & Karplus, M., Eds.) June 25–27, p 23, National Institutes of Health, Bethesda, MD.

Elber, R., & Karplus, M., (1990) *J. Am. Chem. Soc. 112*, 9161–75.

Evans, S. V., & Brayer, G. D. (1988) *J. Biol. Chem. 263*, 4263–8.

Evans, S. V., & Brayer, G. D. (1990) *J. Mol. Biol. 213*, 885–97.

Hendrickson, W. A., & Konnert, J. H. (1979) in *Biomolecular Structure, Conformation, Function and Evolution* (Srinivasan, R., Ed.) Vol. 1, pp 43–57, Pergamon, New York.

Hoard, J. L., Hamor, M. J., Hamor, T. A., & Caughey, W. S. (1965) *J. Am. Chem. Soc. 87*, 2312–8.

Hubbard, S. R., Hendrickson, W. A., Lambright, D. G., & Boxer, S. G. (1990) *J. Mol. Biol. 213*, 213–8.

Johnson, K. A., Olson, J. S., & Phillips, G. N., Jr. (1989) *J. Mol. Biol. 207*, 459–63.

Jones, T. A. (1978) *J. Appl. Crystallogr. 11*, 268–72.

Koenig, D. F. (1965) *Acta Crystallogr. 18*, 663–7.

Kottalam, J., & Case, D. A. (1988) *J. Am. Chem. Soc. 110*, 7690–7.

Kuriyan, J. (1986) Ph.D. Thesis, Massachusetts Institute of Technology, Cambridge, MA.

Kuriyan, J., Wilz, S., Karplus, M., & Petsko, G. A. (1986) *J. Mol. Biol. 192*, 133–54.

La Mar, G. N., Hauksson, J. B., Dugad, L. B., Liddell, P. A., Venkataramana, N., & Smith, K. (1991) *J. Am. Chem. Soc. 113*, 1544–50.

Lambright, D. G., Balasubramanian, S., & Boxer, S. G. (1989) *J. Mol. Biol. 207*, 289–99.

Lecomte, J. T. J., & La Mar, G. N. (1985) *Biochemistry 24*, 7388–95.

Ozaki, Y., Kitigawa, T., & Kyogoku, Y. (1976) *FEBS Lett. 62*, 369–72.

Phillips, S. E. V. (1980) *J. Mol. Biol. 142*, 531–54.

Phillips, G. N., Jr., Arduini, R. M., Springer, B. A., & Sligar, S. G. (1990) *Proteins 7*, 358–65.

Ramachandran, G. N., Ramakrishnan, C., & Sasisekharan, V. (1963) *J. Mol. Biol. 7*, 95–9.

Ringe, D., Petsko, G. A., Kerr, D. E., & Ortiz de Montellano, P. R. (1984) *Biochemistry 23*, 2–4.

Scheidt, W. R., & Chipman, D. M. (1986) *J. Am. Chem. Soc. 108*, 1163–7.

Smerdon, S. J., Oldfield, T. J., Dodson, E. J., Dodson, G. G., Hubbard, R. E., & Wilkinson, A. J. (1990) *Acta Crystallogr. B46*, 370–7.

Smerdon, S. J., Dodson, G. G., Wilkinson, A. J., Gibson, Q. H., Blackmore, R. S., Carver, T. E., & Olson, J. S. (1991) *Biochemistry 30*, 6252–60.

Takano, T. (1977) *J. Mol. Biol. 110*, 537–68.

Waller, D. A., & Liddington, R. C. (1990) *Acta Crystallogr. B46*, 409–18.

Registry No. Fe, 7439-89-6; Lys, 56-87-1; Ser, 56-45-1; Arg, 74-79-3; heme, 14875-96-8.